934 *Inorg. Chem.* **2010**, *49*, 934–942
DOI: 10.1021/ic901668u

Inorganic Chemistry
Article

Jahn−Teller Distorted Frameworks and Magnetic Order in the Rb−Mn−P−O System

Fiona C. Coomer, Neal J. Checker, and Adrian J. Wright*

School of Chemistry, University of Birmingham, Edgbaston, Birmingham B15 2TT, U.K.

Received August 20, 2009

Two previously uncharacterized members of the Rb−Mn−P−O system, $RbMnP_2O_7$ and β-$RbMnHP_3O_{10}$, have been synthesized using a phosphoric acid flux synthetic route and their crystal and magnetic structures determined using neutron powder diffraction. The crystal structure of $RbMnP_2O_7$ (space group $P2_1/c$, $a = 7.3673(2)$ Å, $b = 9.6783(2)$ Å, $c = 8.6467(2)$ Å, and $\beta = 105.487(1)°$) was found to be isostructural with $RbFeP_2O_7$. The polymorph β-$RbMnHP_3O_{10}$ was also isolated as a single phase and found to crystallize in the space group $C2$ ($a = 12.2066(5)$ Å, $b = 8.5243(3)$ Å, $c = 8.8530(4)$ Å, $\beta = 107.233(2)°$). Both structures consist of frameworks of corner-sharing MnO_6 octahedra linked together by condensed phosphate anions, with Rb^+ cations located in the intersecting channels. In both cases the Mn^{3+} octahedra exhibit unusual Jahn−Teller distortions indicative of a plasticity effect driven by the steric requirements of the condensed phosphate anions, and this causes a strong violet coloration similar to that observed in the manganese violet pigment; the structure of this has yet to be determined. Magnetic susceptibility measurements show that both $RbMnP_2O_7$ ($T_N = 20$ K) and β-$RbMnHP_3O_{10}$ ($T_N = 10$ K) undergo a phase transition at low temperatures to an antiferromagnetically ordered state. Low-temperature neutron powder diffraction studies show that the magnetic ground states of each of these materials involve both ferromagnetic and antiferromagnetic super-superexchange interactions between orbitally ordered Mn^{3+}, which are mediated by PO_4 tetrahedra. These interactions are compared and discussed.

Introduction

The huge variety of known and potential inorganic framework materials offers an opportunity to explore fundamental materials chemistry and to develop materials displaying a range of diverse and exploitable properties. This has driven much research in recent years and has led to the discovery of many new systems, including those based on purely inorganic frameworks (e.g., metal phosphate zeotypes)[1] and, more recently, the hybrid metal−organic frameworks (MOFs).[2] Significant progress has also been made in harnessing their potential, as exemplified by the development of materials whose open framework structures can be tailored to control and catalyze organic reactions.[3]

The presence of transition-metal ions within a framework can offer a number of potentially important properties, including catalytic, optical, conducting, and magnetic behavior.[4,5] A rich area of relatively unexplored framework possibilities may be found in transition-metal condensed phosphate systems. The simplest condensed phosphate anion is diphosphate (or pyrophosphate, $P_2O_7^{4-}$), which is adaptive to the bonding requirements within a structure, principally through variations in the P−O−P bond angle. This leads to significant structural diversity in transition-metal diphosphate systems, as evident in $A^{I}M^{III}P_2O_7$ (A^{I} = alkali metal, M^{III} = V, Fe, Mo),[6,7] where the framework consists of corner-sharing MO_6 octahedra and P_2O_7 units. Similarly, although less studied, triphosphate anions ($P_3O_{10}^{5-}$) are known to form frameworks with transition metals,[8−12] providing further examples of metal−phosphate framework topologies.

Framework materials possessing magnetic order are relatively rare but are of fundamental interest in understanding the nature of magnetic interactions. To this end, we have identified the Rb−Mn−P−O condensed phosphate system,

*To whom correspondence should be addressed. E-mail: a.j.wright@bham.ac.uk. Tel: +44 121 414 4406. Fax: +44 121 414 4403.

(1) Hix, G. B. *Annu. Rep. Prog. Chem., Sect. A: Inorg. Chem.* **2005**, *101*, 394–428.
(2) Rosseinsky, M. J. *Microporous Mesoporous Mater.* **2004**, *73*(1−2), 15–30.
(3) Thomas, J. M. *Angew. Chem., Int. Ed.* **1999**, *38*(24), 3588–3628.
(4) Murugavel, R.; Choudhury, A.; Walawalkar, M. G.; Pothiraja, R.; Rao, C. N. R. *Chem. Rev.* **2008**, *108*(9), 3549–3655.
(5) Natarajan, S.; Mandal, S. *Angew. Chem., Int. Ed.* **2008**, *47*(26), 4798–4828.
(6) Dvoncova, E.; Lii, K.-H. *J. Solid State Chem.* **1993**, *105*(1), 279–286.
(7) Millet, J. M. M.; Mentzen, B. F. *Eur. J. Solid State Inorg. Chem.* **1991**, *28*(3−4), 493–504.
(8) Guesdon, A.; Daguts, E.; Raveau, B. *J. Solid State Chem.* **2002**, *167*(1), 258–264.
(9) Rishi, S. K.; Kariuki, B. M.; Checker, N. J.; Godber, J.; Wright, A. J. *Chem. Commun.* **2006**, No. 7, 747–749.
(10) Wright, A. J.; Attfield, J. P. *J. Solid State Chem.* **1998**, *141*(1), 160–163.
(11) Wright, A. J.; Ruiz-Valero, C.; Attfield, J. P. *J. Solid State Chem.* **1999**, *145*(2), 479–483.
(12) Wright, A. J.; Attfield, J. P. *Inorg. Chem.* **1998**, *37*, 3858–3861.

 Published on Web 12/30/2009

in particular phases containing Mn^{3+}, as offering an important insight into frameworks possessing orbital order via Jahn−Teller distortions and their influence on magnetic order. This system was first investigated in 1988 by Guzeeva and Tananaev,[13] who identified a number of distinct phases, including $RbMnP_2O_7$ and two polymorphs of $RbMnHP_3O_{10}$ (previously labeled I and II, hereafter referred to as α and β, respectively, for consistency with the standard polymorph labeling), and reported their syntheses and X-ray powder diffraction patterns but provided no further structural details. Previous studies by Wright and Attfield[12] have solved the nuclear and magnetic structure of α-$RbMnHP_3O_{10}$. Here we report for the first time the nuclear and magnetic structures of two further phases from the Rb−Mn−P−O system, β-$RbMnHP_3O_{10}$ and $RbMnP_2O_7$, enabling a detailed comparison with related frameworks containing Mn^{3+} and allowing the further investigation of exchange interactions between orbitally ordered Mn^{3+} ions mediated through phosphate linkages. While exchange interactions via a single intervening diamagnetic species (superexchange) are now readily predicted (via Goodenough's[14] and Kanamori's[15] seminal work), descriptions of longer exchange pathways through multiple species (often referred to as super-superexchange) are much less developed. Significantly, the condensed phosphate phases studied here possess magnetic order but are sufficiently magnetically dilute to provide further examples of these longer range magnetic interactions.

Experimental Section

$RbMnP_2O_7$ and β-$RbMnHP_3O_{10}$ were prepared using a method similar to that for α-$RbMnHP_3O_{10}$,[12] via a classic phosphoric acid melt method using a solution of Rb_2CO_3 and Mn_2O_3 in H_3PO_4 (85 wt %). These two different phases could each be isolated by varying only the Rb:Mn ratio in the reaction mixture; varying the pH was found not to affect the favored product. β-$RbMnHP_3O_{10}$ is synthesized when the molar ratio of reagents Rb:Mn:P is in the range (7−7.5):1:15. The optimized ratio was found to be 7:1:15, which was used to synthesize the sample reported in this paper. $RbMnP_2O_7$ can be synthesized using the reagents in a molar ratio Rb:Mn:P of (9−10):1:15, with the optimized ratio of reagents used to produce the sample reported in this paper being 9:1:15. In each case, the solution was heated at 250 °C for 48 h before it was cooled to room temperature over a 24 h period. For both phases, the product was then collected by suction filtration and washed with water, yielding a purple microcrystalline powder in each case.

Initial sample characterization was performed on a Siemens D5000 powder X-ray diffractometer. Neutron powder diffraction data were recorded on the HRPT instrument at SINQ, Paul Scherrer Institute, Switzerland, using an incident neutron wavelength of 1.886 Å, over the range $10 \le 2\theta \le 140°$, for 8 h per data set, at temperatures of 2 and 100 K. Rietveld analyses[16] of the neutron diffraction data were carried out using the GSAS software package[17] to refine both the nuclear and magnetic structures of these phases. The refinements performed used a linear interpolated background function and an asymmetry corrected pseudo Voigt peak shape.[18]

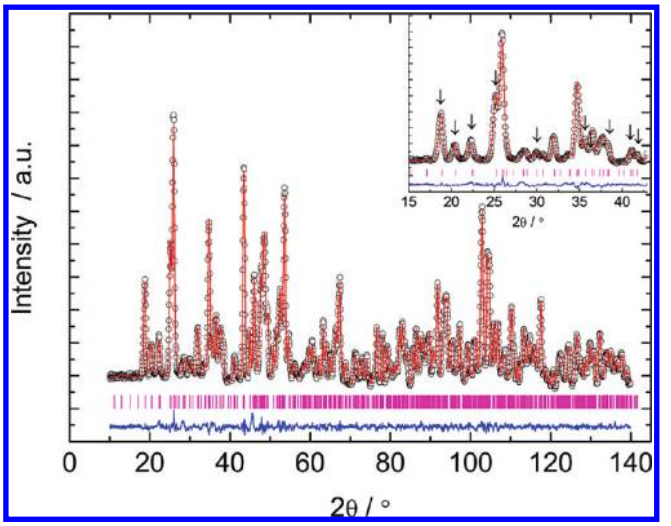

Figure 1. Observed (○), calculated (red line), and difference (blue line) profiles and reflection positions (magenta marks) of the Rietveld refinement carried out on the neutron diffraction data measured on $RbMnP_2O_7$ at 2 K. The low-angle region is enlarged in the inset, with arrows indicating peaks with significant magnetic intensity.

The magnetic susceptibility measurements of $RbMnP_2O_7$ were carried out using a Quantum Design Physical Properties Measurement System (PPMS), using 73.9 mg of sample. The ACMS control system was set up in DC extraction mode, which mimics the SQUID detection system. The magnetic susceptibility of β-$RbMnHP_3O_{10}$ was measured on a Quantum Design Magnetic Properties Measurement System (MPMS), using 66.9 mg of sample. In both cases zero-field-cooled (ZFC) and field-cooled (FC) measurements were carried out under an applied field of 0.1 T. No differences were observed between ZFC and FC measurements, and therefore only ZFC measurements are reported here.

Results and Discussion

$RbMnP_2O_7$. Crystal Structure. The X-ray powder diffraction pattern of $RbMnP_2O_7$ was initially indexed using 25 accurately measured reflection peak positions using the Treor program.[19] This resulted in a primitive monoclinic cell with parameters similar to those reported for $RbFeP_2O_7$,[7] and therefore this structure was used as an initial model for $RbMnP_2O_7$ in Rietveld refinements of the neutron diffraction data measured at both 100 and 2 K. The refinement of the 100 K data converged to a value of $wR_p = 2.20\%$, confirming $RbMnP_2O_7$ adopts a structure with space group $P2_1/c$ and unit cell parameters $a = 7.3708(1)$ Å, $b = 9.6773(2)$ Å, $c = 8.6494(2)$ Å, and $\beta = 105.462(1)°$. There is no evidence of a structural phase transition on cooling to 2 K, and the data yielded the cell parameters $a = 7.3673(2)$ Å, $b = 9.6783(2)$ Å, $c = 8.6467(2)$ Å, $\beta = 105.487(1)°$, and $wR_p = 2.24\%$ (see Figure 1). The final refined structural parameters are shown in Table 1, and selected bond lengths and angles are given in Table 2.

The resulting nuclear structure (see Figure 2) consists of intersecting framework tunnels, with the 10-coordinate Rb^+ ions located at the intersection of these tunnels. The framework consists of Jahn−Teller distorted MnO_6 octahedra corner sharing with P_2O_7 groups. The Mn^{3+} are octahedrally coordinated but do not show a simple tetragonal [4 + 2]

(13) Guzeeva, L. S.; Tananaev, I. V. *Inorg. Mater.* **1988**, *24*(4), 538–542.
(14) Goodenough, J. B. *Phys. Rev.* **1955**, *100*(2), 564–573.
(15) Kanamori, J. *J. Phys. Chem. Solids* **1959**, *10*(2−3), 87–98.
(16) Rietveld, H. M. *Acta Crystallogr.* **1967**, *22*, 151.
(17) Larson, A. C.; von Dreele, R. B. *General Structure Analysis System (GSAS)*; Los Alamos National Laboratory Report LAUR, **2000**; pp 86−748.
(18) Thompson, P.; Cox, D. E.; Hastings, J. B. *J. Appl. Crystallogr.* **1987**, *20*, 79–83.
(19) Werner, P.-E.; Eriksson, L.; Westdahl, M. *J. Appl. Crystallogr.* **1985**, *18*(Oct), 367–370.

Table 1. Refined Structural Parameters for $RbMnP_2O_7$ Obtained from Rietveld Analysis of Neutron Diffraction Data Measured at 2 K (Space Group $P2_1/c$)[a]

atom	site	occupancy	x	y	z	$100U_{iso}/Å^2$
Mn	4*e*	1.0	0.2294(6)	0.6031(5)	0.7563(6)	0.82(9)
Rb	4*e*	1.0	0.1806(3)	0.3119(3)	0.0437(3)	1.36(7)
P(1)	4*e*	1.0	0.4373(4)	0.6306(3)	0.1904(3)	1.21(8)
P(2)	4*e*	1.0	0.1322(4)	0.9059(3)	0.8307(4)	0.95(7)
O(1)	4*e*	1.0	0.3327(5)	0.9501(3)	0.8056(4)	1.21(7)
O(2)	4*e*	1.0	0.0868(4)	0.7380(3)	0.2558(3)	1.58(8)
O(3)	4*e*	1.0	0.6354(4)	0.5756(3)	0.2357(4)	1.46(7)
O(4)	4*e*	1.0	0.1435(4)	0.5904(3)	0.5043(3)	1.39(7)
O(5)	4*e*	1.0	0.3263(4)	0.6043(3)	0.0204(3)	1.51(7)
O(6)	4*e*	1.0	0.9885(4)	0.4967(3)	0.2268(3)	1.13(7)
O(7)	4*e*	1.0	0.4455(5)	0.7841(3)	0.2445(4)	1.26(8)

[a] Lattice parameters: a = 7.3673(2) Å, b = 9.6783(2) Å, c = 8.6467(2) Å, β = 105.487(1)°, V = 594.16(3) Å^3. Magnetic moments: M_x = 0.36(8) μ_B; M_y = 0.0 μ_B; M_z = −3.97(4) μ_B; $|M|$ = 3.99(4) μ_B. R factors: wR_p = 2.24%, R_p = 1.72%, R_{F^2} = 1.92%, χ^2 = 6.915.

Table 2. Selected Bond Distances (Å) and Angles (deg) for $RbMnP_2O_7$ Measured at 2 K

Mn−O(2)	1.861(5)	Mn−O(5)	2.203(5)
Mn−O(3)	1.988(5)	Mn−O(6)	1.913(5)
Mn−O(4)	2.104(6)	Mn−O(7)	1.955(5)
P(1)−O(1)	1.615(5)	P(2)−O(1)	1.607(4)
P(1)−O(3)	1.504(4)	P(2)−O(2)	1.535(5)
P(1)−O(5)	1.501(4)	P(2)−O(4)	1.482(4)
P(1)−O(7)	1.553(4)	P(2)−O(6)	1.519(4)
O(2)−Mn−O(3)	174.8(3)	O(3)−Mn−O(7)	94.6(2)
O(2)−Mn−O(4)	91.9(2)	O(4)−Mn−O(5)	176.7(3)
O(2)−Mn−O(5)	91.4(2)	O(4)−Mn−O(6)	91.3(3)
O(2)−Mn−O(6)	86.1(2)	O(4)−Mn−O(7)	90.2(2)
O(2)−Mn−O(7)	90.3(2)	O(5)−Mn−O(6)	88.3(2)
O(3)−Mn−O(4)	89.7(2)	O(5)−Mn−O(7)	90.5(2)
O(3)−Mn−O(5)	87.0(2)	O(6)−Mn−O(7)	176.2(3)
O(3)−Mn−O(6)	88.9(2)		

Jahn−Teller distortion, as might be expected for a high-spin d^4 ion, but instead display a further distortion. This consists of two long axial bonds (2.20 and 2.10 Å) and a range of shorter bonds, two of medium length (1.99 and 1.96 Å) and two shorter (1.91 and 1.86 Å). It is worth noting here that the "parent" $RbFeP_2O_7$ structure[7] itself also displays a range of Fe−O bond lengths, ranging from 1.92 to 1.99 Å, even though it contains Fe^{3+} (high-spin d^5), rather than Jahn−Teller active Mn^{3+}. It is useful at this point to consider bond valence sum (BVS) calculations,[20] which are commonly used to estimate the oxidation states of atoms from the number of coordinating species and their bond lengths to the atom being considered. For Mn^{3+} in our structure, a BVS of +3.25 was obtained, which is consistent with this valency, albeit slightly overbonded. If we now consider the pyrophosphate group, which displays typically distorted PO_4 tetrahedra, with long P−O bonds to the bridging O(1) atom and shorter bonds to terminal O atoms, similar BVS calculations for the two P sites in this structure provide close to ideal values for P^{5+}, with BVS values of +4.9 and +5.0 for P(1) and P(2), respectively. It would therefore appear that the steric requirements imposed by the pyrophosphate ligands as they chelate to the Mn^{3+} ions are dominant and this causes further distortions of the octahedral site. This influence of the local structural environment over electronic

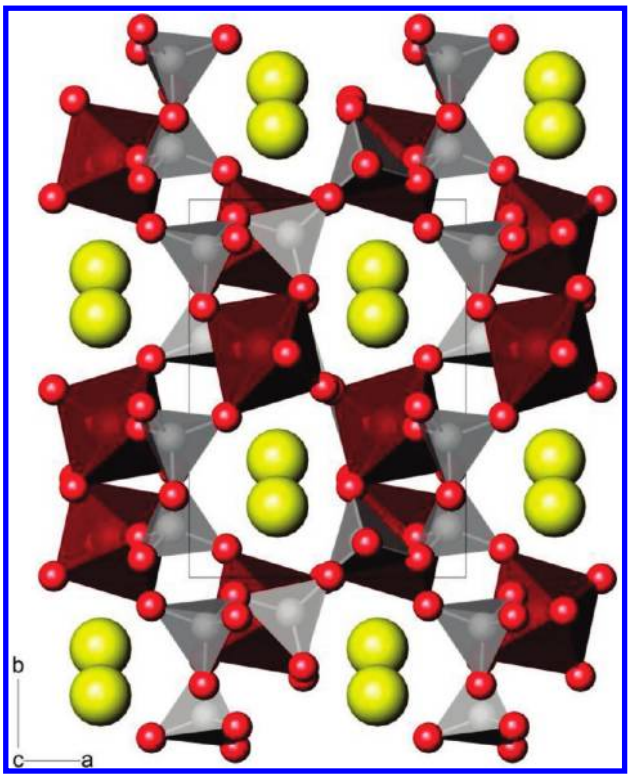

Figure 2. Nuclear structure of $RbMnP_2O_7$ viewed down the c axis, showing MnO_6 octahedra (deep red), Rb^+ ions (yellow), and P_2O_7 condensed phosphate anions (gray). The thin black line defines the unit cell.

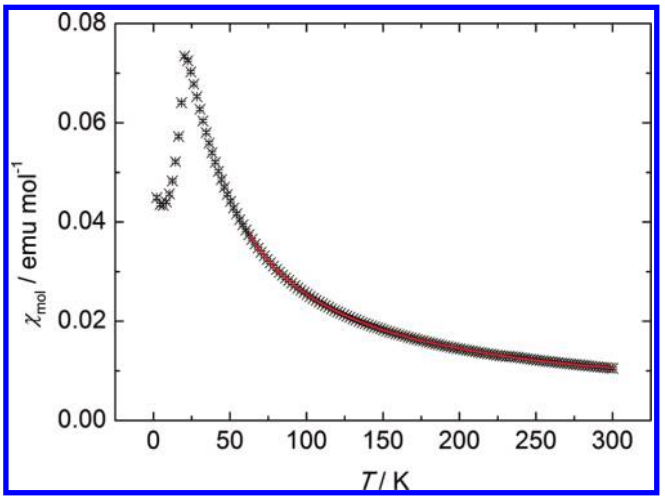

Figure 3. Temperature dependence of the magnetic susceptibility of $RbMnP_2O_7$ (black crosses) with a fit to the Curie−Weiss law (red line).

considerations of the Jahn−Teller active Mn^{3+} has been seen in a number of other systems (e.g., $Mn(acac)_3$[21]) and is known as the plasticity effect, describing the relatively soft (plastic) coordination sphere of the metal in question.[22]

Interestingly, the intense violet color exhibited by $RbMnP_2O_7$ appears similar to that of the commercially available pigment "manganese violet"[23] (nominally $NH_4MnP_2O_7$), and although the structure of this pigment

(20) Brown, I. D.; Altermatt, D. *Acta Crystallogr., Sect. B* **1985**, *41*(Aug), 244–247.

(21) Fackler, J. P.; Avdeef, A. *Inorg. Chem.* **1974**, *13*(8), 1864–1875.

(22) Bersuker, I. B., In *The Jahn-Teller Effect*; Cambridge University Press: Cambridge, U.K., 2005; pp 495−498.

(23) Lee, J. D.; Browne, L. S. *J. Chem. Soc. A* **1968**, No. 3, 559–561.

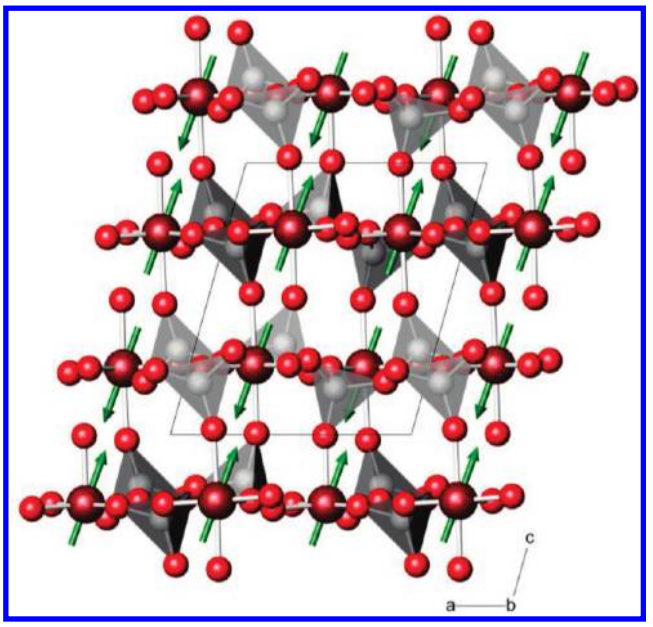

Figure 4. Magnetic structure of $RbMnP_2O_7$ at 2 K viewed down the [010] direction, showing the orientation of the magnetic moments of the Mn^{3+} ions (green arrows).

remains unreported, the distorted manganese coordination is likely to be similar in both materials and should provide some structural insight into the optical behavior of Mn^{3+} pigments.

Magnetic Properties. The magnetic susceptibility data, measured on 73.9 mg of sample (Figure 3), shows that $RbMnP_2O_7$ orders antiferromagnetically with $T_N = 20$ K. At temperatures above this transition temperature it behaves as a Curie−Weiss paramagnet, and a Curie−Weiss curve fitted at $T \geq 50$ K gives the effective magnetic moment $\mu_{eff} = 4.54\,\mu_B$ (cf. 4.9 μ_B expected for high-spin d^4 Mn^{3+} ions[24]) and $\Theta = -10.9(2)$ K. The sharp Néel transition and negative Θ suggest that three-dimensional antiferromagnetic order occurs at temperatures below 20 K. Indeed, as T_N is approximately twice the magnitude of Θ, this suggests that both ferromagnetic and antiferromagnetic pathways are present, and all are satisfied in the long-range ordered arrangement.

After the nuclear contribution was fitted for the 2 K neutron diffraction pattern, extra peaks and intensity were evident (Figure 1, inset). From these a magnetic unit cell was determined, commensurate with the nuclear cell and consistent with the magnetic space group $P2_1'/c$. The magnetic intensities were Rietveld-fitted using a calculated form factor for Mn^{3+}.[25] A good agreement between observed and calculated intensities was obtained (wR_p = 2.24%), with the relative orientations of the four Mn spins in the unit cell found to be (0.23, 0.90, 0.26)+, (0.23, 0.60, 0.76)−, (0.77, 0.40, 0.24)+, and (0.77, 0.10, 0.74)−. The magnitude of the moments was found to be 3.99(4) μ_B, as would be expected for a high-spin Mn^{3+}, and their easy axis was found to be orientated effectively parallel to the *c* axis, a direction closely related to that of the long Mn−O bonds of the Jahn−Teller distorted MnO_6 octahedra (shown in Figure 4).

(24) Carlin, R. L., *Magnetochemistry*; Springer-Verlag: Berlin, 1986.
(25) Brown, P. J. In *International Tables of Crystallography*; Kluwer Academic: Dordrecht, 1992; Vol. *C*.

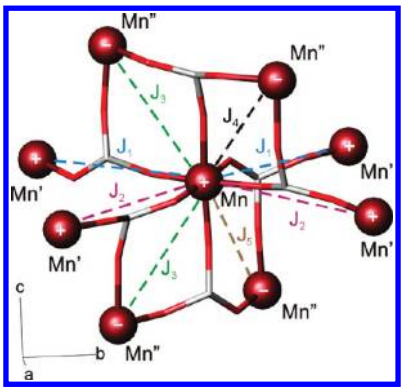

Figure 5. Nearest neighbor Mn−Mn interactions in $RbMnP_2O_7$, with magnetic exchange pathways labeled. Relative spin orientations are indicated by + or −.

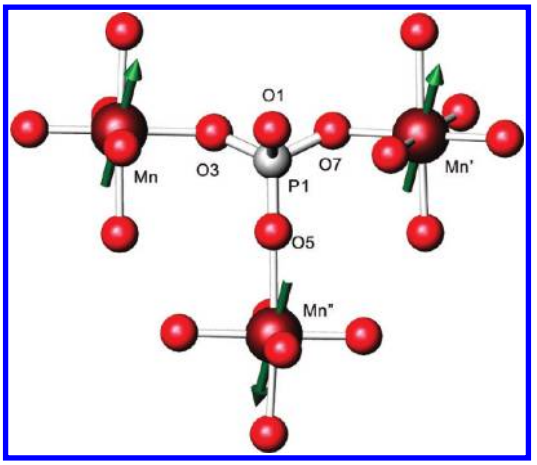

Figure 6. Magnetic exchange pathways in $RbMnP_2O_7$ linking Mn^{3+} ions via the $P(1)O_4$ unit of the P_2O_7 group (Mn−···−Mn′, J_2; Mn−···−Mn″, J_4; Mn′−···−Mn″, J_3). Moment directions are indicated by arrows. A similar situation exists around the other $P(2)O_4$ unit of the P_2O_7 group.

Clearly as Mn−Mn distances within the structure are too long (> 5 Å) to facilitate direct exchange, it is therefore likely that the exchange pathway responsible for the magnetic order at low temperature is facilitated via intervening phosphate tetrahedra. Whangbo et al.[26,27] have considered the nature of many such interactions, often described as super-superexchange interactions, and have identified the O---O separation as being highly significant: the closer this separation, the stronger the interaction. In this structure, the closest Mn−O---O−Mn interactions occur via Mn−O−P−O−Mn linkages (i.e., via an intervening PO_4 tetrahedron), and therefore we shall describe the magnetic interactions using such linkages. Accordingly, each Mn spin is connected to other Mn spins via four apparently ferromagnetic Mn−O−P−O−Mn pathways within the *ab* plane (J_1 and J_2) and four similar but antiferromagnetic pathways in the *c* direction (J_3, J_4, and J_5) (see Figure 5). The shorter Mn−O bonds mediating the ferromagnetic interactions are within the equatorial plane of the Jahn−Teller distorted octahedra, and from crystal field considerations these

(26) Whangbo, M. H.; Dai, D.; Koo, H. J. *Dalton Trans.* **2004**, No. 19, 3019–3025.
(27) Whangbo, M. H.; Koo, H. J.; Dai, D. *J. Solid State Chem.* **2003**, *176*(2), 417–481.

are in the direction of the empty $d_{x^2-y^2}$ orbitals. In contrast, the antiferromagnetic interactions are each mediated by one such short bond and by one long axial Mn−O bond (associated with the singly occupied d_{z^2}). However, on closer inspection of the structure it is clear that each PO_4 unit within the P_2O_7 group simultaneously connects together three Mn centers (nominally Mn, Mn′, and Mn″) via the three oxygens on the terminal triangular faces of the P_2O_7 unit; only the bridging O(1) is not involved (see Figure 6). Thus, the apparent ferromagnetic super-superexchange interactions that occur within the *ab* plane, mediated via the shorter, equatorial Mn−O bonds (J_1 and J_2) are also each connected via P(1)−O(5) and P(2)−O(4) to the axial Mn″−O(5) and Mn″−O(4) bonds, respectively, in an apparent antiferromagnetic super-superexchange interaction (i.e., J_3, J_4, and J_5). This effectively gives a triad of interlinked exchange interactions which define all the spin directions in the structure. Given the similarities in the geometries of the linkages Mn″−···−Mn and Mn″−···−Mn′ (as shown in Figure 6), which all contain a longer apical Mn−O bond and a shorter Mn−O bond with similar bond angles, we might expect these to provide similar exchange interactions. If this is the case, then it rather limits the possible spin scenarios for the triad if we are to observe a simple collinear ordered arrangement. If these aforementioned super-superexchange interactions (i.e., Mn″−···−Mn′ and Mn″−···−Mn) are ferromagnetic, then the remaining super-superexchange interaction (Mn′−···−Mn) is constrained to be ferromagnetic, resulting in a ferromagnetic material. Equally, if both are antiferromagnetic, then this remaining interaction is therefore ferromagnetic, leading to an overall antiferromagnetic material. The magnetic structure obtained from low-temperature neutron data is in accordance with this latter scenario. Clearly, a combination of the geometries, orbital occupancies, and relative strengths of interactions are responsible for the nature of the observed exchange interactions. A further discussion of the general nature of the exchange interactions in $RbMnP_2O_7$ is presented later in this paper when geometries and orbital occupancies are considered alongside those observed in α- and β-$RbMnHP_3O_{10}$.

***β*-$RbMnHP_3O_{10}$. Crystal Structure.** An initial single-crystal X-ray diffraction analysis of a low-quality crystal was able to provide a basic structural model for β-$RbMnHP_3O_{10}$, which was then used in conjunction with a Rietveld refinement of the neutron powder diffraction data to determine the complete structural details.[28] The resulting model was refined, using data measured at 100 K, in the space group *C*2 and converged to a value of $wR_p = 2.50\%$ with unit cell parameters $a = 12.2187(4)$ Å, $b = 8.5226(3)$ Å, $c = 8.8629(3)$ Å, and $\beta = 107.244(2)°$. When the temperature was lowered to 2 K, there was no evidence of any structural phase transition and the refinement converged with $wR_p = 2.79\%$, $a = 12.2066(5)$ Å, $b = 8.5243(3)$ Å, $c = 8.8530(4)$ Å, and $\beta = 107.233(2)°$ (see Figure 7). The final refined structural details are given in Table 3 and selected bond lengths and angles in Table 4.

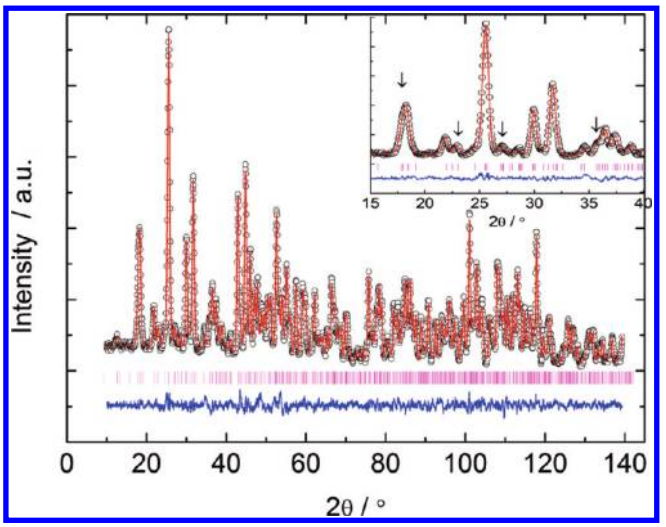

Figure 7. Observed (○), calculated (red line), and difference (blue line) profiles and reflection positions (magenta marks) of the Rietveld refinement carried out on the neutron diffraction data measured on β-$RbMnHP_3O_{10}$ at 2 K. The low-angle region is enlarged in the inset, with arrows indicating peaks with significant magnetic intensity.

Table 3. Refined Structural Parameters for β-$RbMnHP_3O_{10}$ Obtained from Rietveld Analysis of Neutron Diffraction Data Measured at 2 K (Space Group *C*2)[a]

atom	site	occupancy	*x*	*y*	*z*	$100U_{iso}$/Å^2
Rb	4*c*	1.0	0.7654(5)	0.8644(6)	0.2342(7)	0.9(2)
Mn(1)	2*b*	1.0	0	0.187(2)	0.5	0.6(4)
Mn(2)	2*a*	1.0	0	0.716(2)	0	1.2(4)
P(1)	4*c*	1.0	0.9715(7)	0.4894(9)	0.2720(8)	0.2(2)
P(2)	4*c*	1.0	0.7678(8)	0.3026(9)	0.213(1)	0.8(2)
P(3)	4*c*	1.0	0.5747(7)	0.487(1)	0.237(1)	0.7(2)
O(1)	4*c*	1.0	0.9371(6)	0.613(1)	0.368(1)	1.1(2)
O(2)	4*c*	1.0	0.0337(6)	0.5472(8)	0.1571(9)	1.2(2)
O(3)	4*c*	1.0	0.0399(6)	0.3559(9)	0.3687(9)	0.8(2)
O(4)	4*c*	1.0	0.8529(6)	0.4124(7)	0.1555(8)	0.2(2)
O(5)	4*c*	1.0	0.8294(6)	0.1924(9)	0.3274(9)	1.5(2)
O(6)	4*c*	1.0	0.6823(6)	0.2312(8)	0.0594(9)	0.7(2)
O(7)	4*c*	1.0	0.7043(6)	0.424(1)	0.3006(9)	1.3(2)
O(8)	4*c*	1.0	0.4959(5)	0.3626(8)	0.1570(8)	0.1(2)
O(9)	4*c*	1.0	0.5482(6)	0.5344(9)	0.391(1)	1.3(2)
O(10)	4*c*	1.0	0.5797(7)	0.6280(8)	0.130(1)	1.7(2)
H(1)	2*a*	1.0	0	0.130(2)	0	0.9(4)
H(2)	2*b*	1.0	0	0.619(2)	0.5	4.2(6)

[a] Lattice parameters: $a = 12.2066(5)$ Å, $b = 8.5243(3)$ Å, $c = 8.8530(4)$ Å, $\beta = 107.233(2)°$, $V = 879.83(9)$ Å^3. Magnetic moments: $M_x = 3.54(8)\,\mu_B$; $M_y = 0.0\,\mu_B$; $M_z = 1.4(2)\,\mu_B$; $|M| = 3.81(6)\,\mu_B$. *R*-factors: $wR_p = 2.79\%$, $R_p = 2.19\%$, $R_{F^2} = 3.43\%$, $\chi^2 = 6.526$.

The structure of β-$RbMnHP_3O_{10}$ was found to possess the same framework topology as α-$RbMnHP_3O_{10}$,[12] containing MnO_6 octahedra which are linked by hydrogen triphosphate anions to produce a three-dimensional framework with Rb^+ cations situated within the framework channels. A polyhedral representation of the structure of β-$RbMnHP_3O_{10}$ is shown in Figure 8. Both polymorphs crystallize in *C*-centered monoclinic space groups with very similar lattice parameters, resulting in a difference in density between the two phases of $<1\%$. The loss of the glide plane in β-$RbMnHP_3O_{10}$ results in two formula units per asymmetric unit and two unique Mn environments within the unit cell; this compares with one present in α-$RbMnHP_3O_{10}$ (space group $C2/c$). The

(28) The single-crystal analysis provided accurate lattice parameters, indicated a suitable space group, and provided locations of the heavier scattering Rb, Mn, and P atoms. The remaining atoms in the structure were located from unassigned scattering intensity via Fourier difference mapping generated from the Rietveld analysis of the neutron powder diffraction data.

Table 4. Selected Bond Distances (Å) and Angles (deg) for β-$RbMnHP_3O_{10}$ Measured at 2 K

Mn(1)−O(3)	2.00(2) [×2]	Mn(2)−O(2)	1.96(1) [×2]
Mn(1)−O(5)	2.188(7) [×2]	Mn(2)−O(6)	2.134(7) [×2]
Mn(1)−O(9)	1.82(2) [×2]	Mn(2)−O(8)	1.88(1) [×2]
P(1)−O(1)	1.49(1)	P(3)−O(7)	1.60(1)
P(1)−O(2)	1.52(1)	P(3)−O(8)	1.46(1)
P(1)−O(3)	1.52(1)	P(3)−O(9)	1.55(1)
P(1)−O(4)	1.65(1)	P(3)−O(10)	1.54(1)
P(2)−O(4)	1.59(1)	H(1)−O(10)	1.271(9)
P(2)−O(5)	1.42(1)	H(2)−O(1)	1.193(8)
P(2)−O(6)	1.57(1)	O(1)···O(1′)	2.383(9)
P(2)−O(7)	1.63(1)	O(10)···O(10′)	2.541(9)
Rb−O(1)	2.99(1)	Rb−O(6′)	3.072(9)
Rb−O(2)	3.122(9)	Rb−O(8)	3.086(9)
Rb−O(3)	3.31(1)	Rb−O(9)	3.62(1)
Rb−O(4)	3.347(9)	Rb−O(9′)	3.71(1)
Rb−O(5)	2.954(9)	Rb−O(10)	2.968(9)
Rb−O(6)	3.503(9)		
O(3)−Mn(1)−O(3′)	87.9(8)	O(2)−Mn(2)−O(2′)	85.4(8)
O(3)−Mn(1)−O(5)	85.6(5)	O(2)−Mn(2)−O(6)	83.4(4)
O(3)−Mn(1)−O(5′)	92.6(5)	O(2)−Mn(2)−O(6′)	101.8(5)
O(3)−Mn(1)−O(9)	92.0(3)	O(2)−Mn(2)−O(8)	90.6(3)
O(3)−Mn(1)−O(9′)	175.3(3)	O(2)−Mn(2)−O(8′)	165.2(4)
O(5)−Mn(1)−O(5′)	178(1)	O(6)−Mn(2)−O(6′)	173(1)
O(5)−Mn(1)−O(9)	92.1(4)	O(6)−Mn(2)−O(8)	91.8(4)
O(5)−Mn(1)−O(9′)	89.7(5)	O(6)−Mn(2)−O(8′)	83.6(4)
O(9)−Mn(1)−O(9′)	88.5(9)	O(8)−Mn(2)−O(8′)	96.8(9)
O(1)−P(1)−O(2)	115.8(7)	O(5)−P(2)−O(6)	115.9(7)
O(1)−P(1)−O(3)	114.1(6)	O(5)−P(2)−O(7)	107.9(7)
O(1)−P(1)−O(4)	107.2(6)	O(6)−P(2)−O(7)	111.9(7)
O(2)−P(1)−O(3)	108.7(6)	O(7)−P(3)−O(8)	111.7(7)
O(2)−P(1)−O(4)	103.4(6)	O(7)−P(3)−O(9)	102.5(7)
O(3)−P(1)−O(4)	106.8(6)	O(7)−P(3)−O(10)	105.1(6)
O(4)−P(2)−O(5)	111.0(7)	O(8)−P(3)−O(9)	109.6(6)
O(4)−P(2)−O(6)	106.4(7)	O(8)−P(3)−O(10)	114.3(7)
O(4)−P(2)−O(7)	103.1(5)	O(9)−P(3)−O(10)	112.9(7)
O(10)−H(1)−(10′)	178(2)	O(1)−H(2)−O(1′)	175(2)

framework topology of these polymorphs is also the same as that observed in $CsMnHP_3O_{10}$, and therefore it is possible to compare how the framework adapts to the size of the alkali-metal cations. The structures of $CsMnHP_3O_{10}$ and β-$RbMnHP_3O_{10}$ are both described by the *C*2 space group symmetry, but the latter possesses a unit cell of twice the volume. It would appear that the larger cell is necessary to describe the distortion of the structure to accommodate the smaller Rb, most evident in the ordered displacements of Rb cations within the framework channels.

One of the most prominent structural differences between the two $RbMnHP_3O_{10}$ polymorphs is the differences in pore dimensions. This is evident in their [010] projections (see Figure 8), with the previously reported α-$RbMnHP_3O_{10}$[12] possessing pores with approximate dimensions ∼1.9 × ∼4 Å, whereas the β-$RbMnHP_3O_{10}$ framework undergoes a distortion whereby two pores of different dimension are created; a significantly wider pore (∼2.5 × ∼3.9 Å) alternating with a longer narrower pore (∼1 × ∼4.8 Å). This enlargement of one channel coupled with the narrowing of the adjacent channel appears to be related to a significant rotation of the $Mn(1)O_6$ octahedra around a diad.

In β-$RbMnHP_3O_{10}$, both Mn atoms in the asymmetric unit are located on diads, whereas the Mn site in α-$RbMnHP_3O_{10}$ lies on an inversion center, giving the Mn atoms in the two structures differing coordination geometries. In both α- and β-$RbMnHP_3O_{10}$, the Mn atoms are coordinated by four different triphosphate groups; in β-$RbMnHP_3O_{10}$ the two singularly connected triphosphate groups are found in a cis configuration, whereas in α-$RbMnHP_3O_{10}$ the point symmetry of the Mn atom constrains them to be in a trans configuration.

Table 4 indicates that β-$RbMnHP_3O_{10}$ contains highly distorted MnO_6 octahedra and PO_4 tetrahedra. The MnO_6 octahedra display a marked [2 + 2 + 2] Jahn−Teller distortion with two long axial Mn−O bonds (2 × ∼2.2 Å) and two short (2 × ∼1.85 Å) and two intermediate (2 × ∼1.98 Å) equatorial bonds. This pattern of Mn−O bond lengths is similar to those previously reported for $CsMnHP_3O_{10}$ (low-temperature neutron data)[10] and α-$RbMnHP_3O_{10}$,[12] although in the latter the [2 + 2 + 2] distortion is less pronounced with the four shorter Mn−O lengths more closely matched (2 × 1.92(1) Å, 2 × 1.98(1) Å, 2 × 2.21(1) Å). BVS calculations for Mn^{3+} in β-$RbMnHP_3O_{10}$ give valences of +3.3 for both of the Mn sites, which suggests a less than optimal coordination environment for Mn^{3+}. However, just as was evident with $RbMnP_2O_7$, the BVS calculations for the P in the triphosphate groups are close to optimum (P(1), +4.9; P(2), +4.9; P(3), +5.0), which suggests that the coordination preferences of the triphosphate groups are dominant. These triphosphate groups contain three distorted PO_4 tetrahedra, with longer P−O bonds to the bridging O(4,7) atoms and shorter bonds to the terminal and P−OH oxygen atoms. This pattern of P−O bond lengths is also found in both α-$RbMnHP_3O_{10}$ and $CsMnHP_3O_{10}$. The Rb^+ is in 11-fold coordination (see Table 4), although two of these Rb−O distances are long (> 3.6 Å): cf. the 10-fold coordination exhibited by the alkali-metal cations in α-$RbMnHP_3O_{10}$ and $CsMnHP_3O_{10}$ structures. In all these structures, strong symmetric O···H···O hydrogen bonding links the triphosphate anions into chains, forming the three-dimensional framework. Such hydrogen bonding is common to many hydrogen phosphates.[29]

The difference in Mn^{3+} geometries between the two polymorphs gives rise to a striking difference in observed color: β-$RbMnHP_3O_{10}$ is a deep purple shade, whereas α-$RbMnHP_3O_{10}$ is pale beige. Similarly, $CsMnHP_3O_{10}$ displays a violet color, as does $RbMnP_2O_7$. It is interesting to note that two of the three phases displaying the violet color have Mn located on diads; the other ($RbMnP_2O_7$) has Mn on a general position. These phases also all possess at least one unusually short Mn−O bond (< 1.89 Å). In contrast, α-$RbMnHP_3O_{10}$, which displays a pale beige color, has Mn on an inversion center and all bonds are longer than 1.92 Å. It is therefore clear that the plasticity of the Mn^{3+} coordination in the presence of these condensed phosphate anions provides an opportunity to provide significant variation in optical properties. A more detailed investigation into the optical properties of these materials, particularly their relationship to violet manganese pigments, is currently being undertaken and will be reported elsewhere.

Magnetic Properties. The magnetic susceptibility data, measured using 66.9 mg of sample (Figure 9), show that β-$RbMnHP_3O_{10}$ orders antiferromagnetically below

(29) Emsley, J. *Chem. Soc. Rev.* **1980**, *9*(1), 91–124.

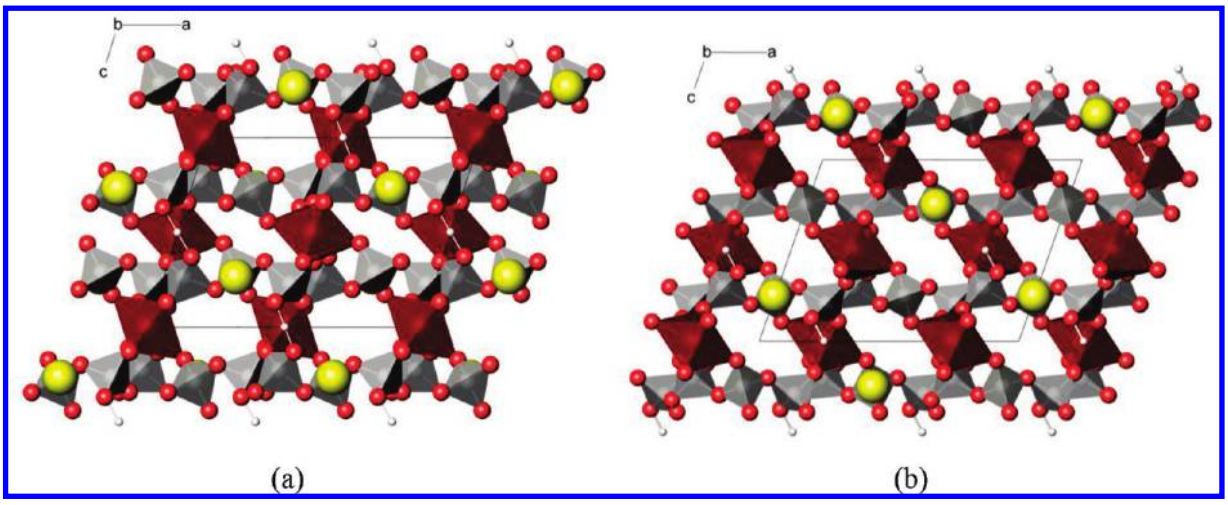

Figure 8. Nuclear structures of (a) β-$RbMnHP_3O_{10}$ and (b) α-$RbMnHP_3O_{10}$ viewed down the *b* axis, showing MnO_6 octahedra (deep red), Rb^+ cations (yellow), H^+ (small white spheres), and P_3O_{10} condensed phosphate anions (gray), with the unit cells outlined.

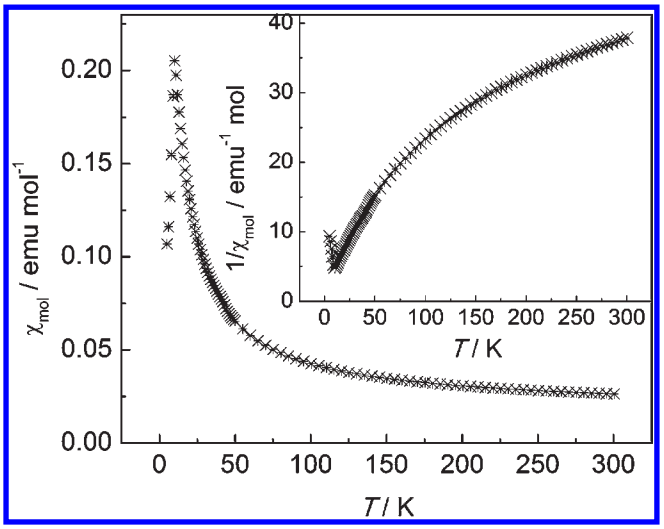

Figure 9. Temperature dependence of the magnetic susceptibility of β-$RbMnHP_3O_{10}$ and inverse susceptibility (inset).

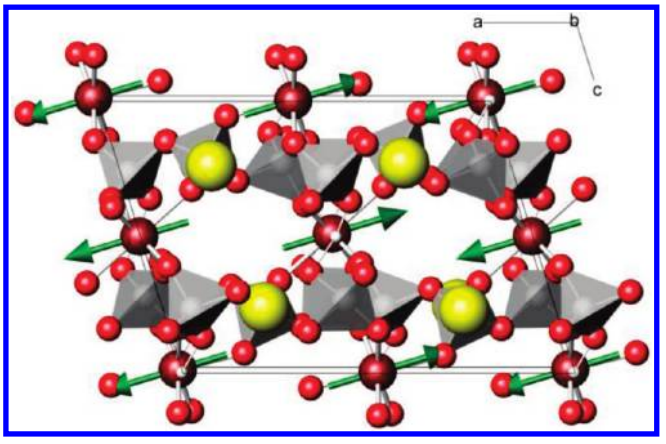

Figure 10. Magnetic structure of β-$RbMnHP_3O_{10}$ at 2 K viewed down the [010] direction, showing the orientation of the magnetic moments of the Mn^{3+} ions (green arrows).

T_N = 10 K, with no deviation between zero-field and field-cooled data. The sharpness of the peak suggests that three-dimensional ordering occurs at this temperature. This transition occurs at a temperature similar to those observed in both $CsMnHP_3O_{10}$ and α-$RbMnHP_3O_{10}$. At higher temperatures it behaves like a paramagnet, but a plot of χ^{-1} vs. *T* data (inset to Figure 9) displays a continuous curvature and no evidence of a linear relationship, thus indicating a marked deviation from ideal Curie−Weiss behavior. It is therefore apparent that the magnetic interactions of the Mn^{3+} ions in β-$RbMnHP_3O_{10}$ are more complex than have been previously observed in either $CsMnHP_3O_{10}$ or α-$RbMnHP_3O_{10}$.

When the nuclear contribution was fitted to the 2 K neutron diffraction pattern, additional magnetic peaks were evident. These magnetic peaks were indexed on the same unit cell as the nuclear structure, with the magnetic space group $Pc2'$. A good agreement between observed and calculated intensities was obtained, with the final refined structural parameters shown in Table 3.

The relative directions of the four Mn spins in the magnetic unit cell were found to be (0, 0.19, 0.5)+, (0, 0.13, 0)+, (0.5, 0.69, 0.5)−, and (0.5, 0.63, 0)−, as shown in Figure 10. This magnetic structure is similar to those previously reported for both α-$RbMnHP_3O_{10}$ and $CsMnHP_3O_{10}$, with the moments directed in the *ac* plane and closely orientated to the direction of the long axial Mn−O bonds of the Jahn−Teller distorted octahedra. The refined magnitude of the Mn^{3+} moments was found to be 3.73(5) μ_B (Figure 7), which is similar to those previously observed for the same ion in α-$RbMnHP_3O_{10}$ (3.82(6) μ_B),[12] $RbMnP_2O_7$ (3.99(4) μ_B), and the low temperature moment observed in $Mn(acac)_3$ (3.8 μ_B).[30]

Within the β-$RbMnHP_3O_{10}$ structure, the Mn ions are situated too far apart (>6 Å) for any significant direct exchange to take place. As discussed previously for $RbMnP_2O_7$ and reported for $CsMnHP_3O_{10}$ and α-$RbMnHP_3O_{10}$, Mn−O−P−O−Mn linkages mediate the magnetic exchange interactions between the Mn ions, resulting in both antiferromagnetic and ferromagnetic exchange interactions within the magnetic structure. In β-$RbMnHP_3O_{10}$, each Mn ion is connected to six other Mn ions, with four of the interactions within the *bc* plane

(30) Gregson, A. K.; Doddrell, D. M.; Healy, P. C. *Inorg. Chem.* **1978**, *17*(5), 1216–1219.

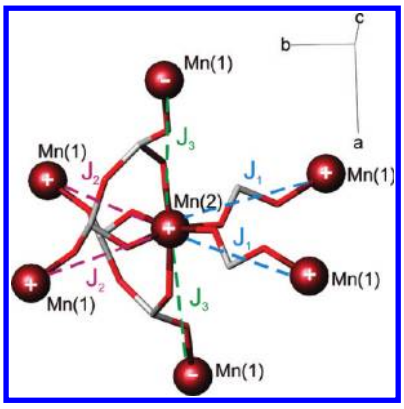

Figure 11. Nearest neighbor Mn−Mn interactions in β-$RbMnHP_3O_{10}$, with magnetic exchange pathways labeled. Relative spin orientations are indicated by + or −.

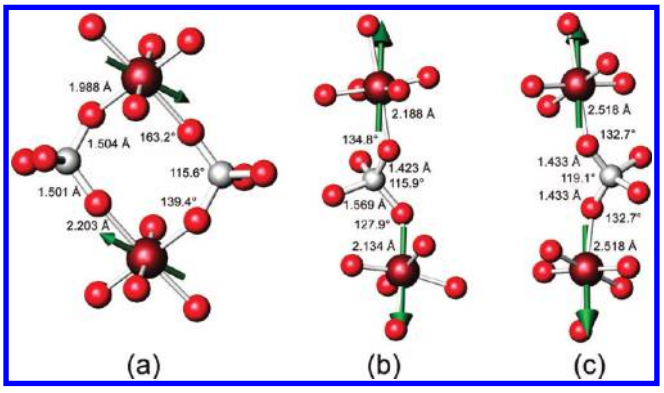

Figure 12. Geometry of antiferromagnetic exchange pathways in (a) $RbMnP_2O_7$, (b) β-$RbMnHP_3O_{10}$, and (c) α-$RbMnHP_3O_{10}$.

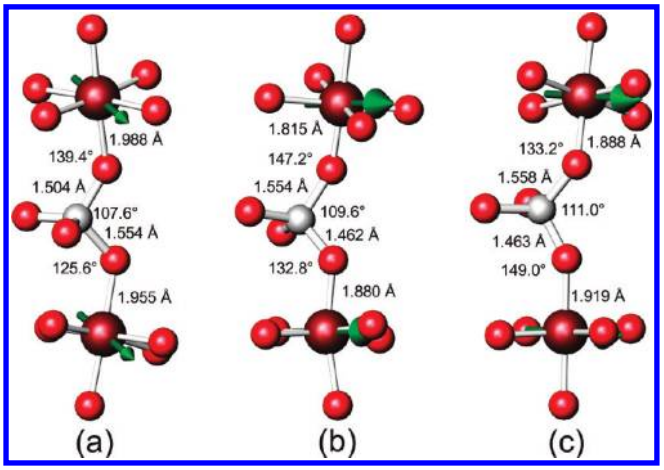

Figure 13. Geometry of ferromagnetic exchange pathways in (a) $RbMnP_2O_7$, (b) β-$RbMnHP_3O_{10}$, and (c) α-$RbMnHP_3O_{10}$.

via two Mn(1)−O(3)−P(1)−O(2)−Mn(2) (J_1) and two Mn(1)−O(9)−P(3)−O(8)−Mn(2) (J_2) linkages. These interactions are all apparently ferromagnetic and provide ferromagnetically ordered layers in the *bc* plane (see Figure 11). The other two connections are in the *a* direction, through antiferromagnetic Mn(1)−O(5)−P(2)−O(6)−Mn(2) (J_3) linkages; hence, the ferromagnetic planes alternate in an antiferromagnetic manner along the *a* direction (see Figure 10). A closer inspection of the magnetic structure indicates that neither the antiferromagnetic nor the ferromagnetic interactions are sufficient on their own to define all the spin directions in this structure. This suggests that the structure is not just a result of one dominant exchange type but that the presence of both types of exchange is real and is derived from the individual exchange pathways. A detailed view of these individual magnetic exchange pathways highlights their similarities to those observed in α-$RbMnHP_3O_{10}$, $RbMnP_2O_7$ (see Figures 12 and 13) and also $CsMnHP_3O_{10}$. The antiferromagnetic exchange interactions involve two long Mn−O bonds, and as the tetragonal Jahn−Teller distortion of a d^4 ion will favor the occupation of the d_{z^2} orbital over the $d_{x^2-y^2}$ orbital, then interactions in the direction of these bonds will involve the singly occupied Mn orbitals. It is interesting to note that if we consider simple superexchange involving these Mn orbitals via a single intervening O (i.e., Mn−O−Mn, as present in ternary manganese oxides) and invoke Goodenough−Kanamori rules,[14,15] then for bond angles of $>100°$ we would expect antiferromagnetic coupling. Clearly in β-$RbMnHP_3O_{10}$ we have a lengthened interaction pathway, with Mn−O---O−Mn separated by ~2.5 Å via an intervening PO_4 group, but we also observe an antiferromagnetic exchange interaction. In contrast, all the nominally ferromagnetic interactions are mediated by two short Mn−O bonds, separated (i.e., Mn−O---O−Mn) by <2.5 Å. In this case, consideration of the Goodenough−Kanamori rules for a simple superexchange interaction involving the interaction of two unoccupied $d_{x^2-y^2}$ orbitals would predict antiferromagnetic coupling. It is therefore apparent that subtle differences in the geometries of these exchange interactions must be influencing the type of exchange observed. A closer examination of the geometry of the O−P−O pathway within the phosphate group shows that, for the ferromagnetic interactions in these materials, the O−P−O angle is $\leq 111.0°$, whereas for the antiferromagnetic interactions, this angle is larger, $>115.5°$, which leads to a slightly extended Mn−O---O−Mn separation. However, this variation in separation is unlikely to be solely responsible for the difference in the sign of the exchange interaction. Fundamentally, it is more likely that subtle changes in the geometry of the exchange interactions change the degree of overlap between adjacent orbitals which facilitate the exchange pathways, much as we see when the M−O−M angle is varied in simple superexchange interactions. Obviously here we have a more complex array of both atomic and molecular orbitals to consider, and at present no clear pattern in behavior has emerged. Further studies are therefore being undertaken to examine these exchange interactions in detail, aided by additional examples from similar magnetically dilute frameworks.

Conclusions

In the Rb−Mn−P−O system we have been able to isolate and structurally characterize two additional phases, β-$RbMnHP_3O_{10}$ and $RbMnP_2O_7$, containing Mn^{3+} in highly distorted coordination environments. These increased levels of distortion, beyond that usually observed for the Jahn−Teller active Mn^{3+}, appears to evidence a plasticity effect, driven by the structural requirements of the condensed phosphate anions. These Mn distortions also appear to

result in an intense violet coloration of the products and suggest similar structural features are adopted by the pigment manganese violet.

A comparison of β-$RbMnHP_3O_{10}$ with the previously reported polymorph α-$RbMnHP_3O_{10}$ shows that they both possess the same framework topology, but the loss of symmetry in β-$RbMnHP_3O_{10}$ allows a distortion to produce markedly dissimilar framework pore dimensions and color.

These condensed phosphate systems provide excellent opportunities to isolate and study magnetically dilute inorganic frameworks which display long-range magnetic order and thus allow the study of magnetic exchange interactions via more than one intervening species. Both $RbMnP_2O_7$ and β-$RbMnP_3O_{10}$ were found to order antiferromagnetically at low temperature, and their magnetic structures were solved by low-temperature neutron powder diffraction. The magnetic structures of $RbMnP_2O_7$, and β-$RbMnHP_3O_{10}$, like that of α-$RbMnHP_3O_{10}$, contain both antiferromagnetic and ferromagnetic exchange interactions, with these interactions mediated through Mn−O−P−O−Mn linkages in which the Mn^{3+} displays ordering of occupied and unoccupied d orbitals. The moments in all three phases align closely with the long, axial direction of the Jahn−Teller distorted MnO_6 octahedra. In $RbMnP_2O_7$, the magnetic structure appears governed by a triad of exchange interactions centered on the terminal faces of the P_2O_7 units, whereas in β-$RbMnHP_3O_{10}$, similar but independent exchange interactions occur. Although these studies have provided more examples of long-range exchange interactions, they have yet to identify a clear pattern or rationale to their behavior and it would appear that further examples of magnetically dilute systems will be required before this can be achieved.

Acknowledgment. We thank the EPSRC (grant EP/E029434/1) for financial support and Dr. D. Sheptyakov for his help with the collection of the neutron diffraction data.